Hindawi
International Transactions on Electrical Energy Systems
Volume 2022, Article ID 7209553, 20 pages
https://doi.org/10.1155/2022/7209553

Research Article

Design and Implementation of Hybrid Transmission Line Protection Scheme Using Signal Processing Techniques

Anup Kumar,[1] Himanshu Sharma,[1] Ram Niwash Mahia,[2] Om Prakash Mahela,[3] and Baseem Khan[4]

[1]*Department of Electrical and Electronics Engineering, SRM Institute of Science and Technology, Ghaziabad, India*
[2]*Department of Electrical Engineering, National Institute of Technology Hamirpur, Hamirpur, India*
[3]*Power System Planning Division, Rajasthan Rajya Vidyut Prasaran Nigam Ltd., Jaipur 302005, India*
[4]*Department of Electrical and Computer Engineering, Hawassa University, Hawassa, Ethiopia*

Correspondence should be addressed to Baseem Khan; baseemkh@hu.edu.et

Received 12 February 2022; Accepted 18 April 2022; Published 10 May 2022

Academic Editor: Akshay Kumar Saha

A hybrid scheme for transmission line protection (HSTLP) using the Stockwell transform (ST), Wigner distribution function (WDF), and alienation coefficient (ACF) is designed. Current signals are analyzed using the ST, WDF, and ACF to compute the Stockwell fault index (SFI), Wigner fault index (WFI), and alienation coefficient fault index (ACFI), respectively. These fault indexes are used to derive a hybrid signal processing fault index (HSPFI), which is implemented for the detection of transmission line fault events. The peak magnitude of HSPFI is compared with a preset threshold magnitude (TH) to identify the fault. The statistical formulation is proposed for fault location on the power transmission line. Fault classification is achieved using the number of faulty phases. A hybrid ground fault index (HGFI) is used to recognize the involvement of the ground during the fault event. This HGFI is determined by processing zero sequence current using ST and WDF. The performance of algorithm is tested by various case studies for fault impedance variation, variable sampling frequency, fault incidence angle variation, reverse power flow on transmission line, highly loaded line, different fault locations online, and noisy conditions. The algorithm is also validated to detect a fault on a practical transmission line of large area utility grid of Rajasthan Rajya Vidyut Prasaran Nigam Limited (RVPN) in India. The algorithm performs better than the Hilbert–Huang transform (HHT)-based protection scheme and wavelet transform (WT)-based protection scheme available in the literature in terms of mean error of fault location, fault location accuracy, and noise level. The proposed protection scheme efficiently detected, classified, and located the faulty events such as single-phase-to-ground fault (SPGF), two-phase fault (TPF), two-phase-to-ground fault (TPGF), three-line fault (TLF), and three-line-to-ground fault (TLGF). Transmission line fault location accuracy of 99.031% is achieved. The algorithm performs well even with a high noise level of 10 dB SNR.

1. Introduction

Fault incident on transmission and distribution lines of the utility grid affects power flow pattern in the network of power system. Transmission line faults lead to interruption in the power flow pattern and sometimes also result in tripping of more elements and affect transient stability, voltage stability, and power system stability [1]. Fast detection and accurate fault location on the transmission line help in fast maintenance and supply restoration, which results in minimum revenue loss and improved power reliability. Machine learning and signal processing techniques have been deployed to design fast and accurate transmission line protection schemes. In [2], the authors designed a protection algorithm for the diagnosis of fault incident on the transmission line by computing the alienation coefficients of current signals. A comparison of samples of post-fault and pre-fault successive current cycles is used to compute alienation coefficients for the detection of fault events. The algorithm is effective to detect faults in a quarter cycle period.

1.1. Related Research Work. A detailed review of techniques used for fault determination and classification is discussed in this section. A fault identification and categorization technique using phase angle variations is reported in [3]. This algorithm used the measurement of instantaneous phase angles of current and voltages computed at both terminals of the line. The discrete Fourier transform (DFT) is applied to compute the derived phase mean index (DPMI) and phase mean index (PMI) of current and voltage associated with all phases of the line. These indexes are utilized for detecting and classifying the fault events considering the global fault detector (GFD) setting. The algorithm effectively detects faults with variations of fault resistances, inception points, power swings, topology changes, load switching, capacitor switching, and even high impedance faults (HIFs). In [4], the authors designed a transmission line protection scheme using the self-attention convolution neural network (SAT-CNN) model for detecting and classifying the faults. The algorithm detected the faults with variations in the voltage and current signals and also considered variable sampling frequencies. A mean error estimation-based protection scheme for the transmission line is reported in [5]. Particle swarm optimization (PSO)-driven optimal threshold setting is used to detect fault events. The algorithm is effective to identify faulty events in the quarter cycle. In [6], the authors designed a fuzzy logic-based protection scheme, which effectively recognizes the series faults and open circuit faults on a six-phase transmission line. The algorithm detected faults for various fault inception angles at different points of the transmission line. A fault detection algorithm using the optimal placement of phasor measurement units (PMUs) is reported in [7]. This is based on the application of positive sequence currents and voltages. The technique is independent of the fault resistance and relies on the admittance. In [8], the authors designed a protection method to recognize and classify the fault events observed on a transmission line compensated by flexible AC transmission system (FACTS) devices. The discrete wavelet transform (DWT) and wavelet entropy computations are implemented for the analysis of current and voltage signals to recognize fault event. This protection technique is simplistic in nature and accurately detects and classifies the fault events. The performance of algorithm is validated using a variety of fault cases. An intelligent technique for the detection and classification of transmission line faults by the use of deep learning technique is reported in [9]. The features are automatically extracted from data of current signals using deep learning to detect fault events. The algorithm is effective to detect fault events in a half cycle. Further, various techniques are recently reported in the literature using pilot superimposed impedance [10], artificial neural network [11], deep learning [12], and wide area measurement [13].

A distance relaying protection scheme for a transmission line compensated by a static synchronous compensator (STATCOM) is introduced by the authors in [14]. This adaptive relying method used the synchronized measurement and effectively identified all faults located on a 300 km transmission line with an accuracy of 0.6%. In [15], the authors proposed a Mho relay algorithm for improving the performance of distance relay installed on transmission line equipped with a static synchronous series compensator (SSSC). This is achieved using a phasor measurement unit (PMU). The algorithm is effective to provide first zone protection to a double-circuit transmission line from single-line-to-ground (SLG) fault. This algorithm is reliable and secure even for changes in the compensation level of SSSC. In [16], the authors addressed the issues pertaining to distance protection of transmission line compensated by STATCOM placed at the midpoint of transmission line. This is achieved using synchronized measurement for adaptive relay setting. It is established that the designed adaptive setting scheme is more accurate, robust, and better than the existing distance protection schemes for STATCOM compensated transmission line. In [17], the authors presented an adaptive distance protection scheme for a transmission line equipped with a static VAR compensator (SVC) at the midpoint of the line. The recursive method is used to mitigate mal-operation of the relays due to the availability of the SVC, and the method performs better relative to the conventional protection method. In [18], the authors presented the calculation of fundamental frequency-based per phase digital impedance pilot relaying (DIPR) scheme for a transmission line compensated by STATCOM. This scheme used the synchronized measurement at both ends of transmission line.

After a detailed analysis of the research reported in this section, a performance comparative study of various signal processing techniques used to design transmission lines is provided in Table 1. This will help to select a technique or combination of techniques to design improved transmission line protection schemes.

1.2. Research Gaps. The detailed review of the techniques discussed in the above paragraph 1.1 indicates that reported techniques use one signal processing method to detect the fault events in the quarter cycle time period and their performance is deteriorated for the noise level higher than 20 dB SNR (signal-to-noise ratio). The performance of fault detection and classification can be improved by the use of two or more signal processing techniques to compute current features. This has been considered as the research focus in this study, and the proposed research work aimed to design a transmission line protection scheme based on current features computed using ST, WDF, and alienation coefficient.

1.3. Research Contribution of Paper. The following are the main research contributions of this study:

(i) Hybridization of ST, WDF, and ACF is used to design a transmission line protection scheme. The current signal is processed by applying the ST, WDF, and ACF to compute the Stockwell fault index (SFI), Wigner fault index (WFI), and alienation coefficient fault index (ACFI), respectively. These indexes are utilized for computing a hybrid signal processing fault index (HSFI) for the detection of fault events.

Table 1: Comparative study of signal processing techniques used to design transmission line protection schemes.

S. no.	Characteristics	Signal processing techniques				
		STFT	WT	ST	WDF	ACF
1	Window size	Fixed	Variable	Adjustable	Variable	Adjustable
2	Parameter measurement (time, frequency, magnitude)	Possible	Possible	Possible	Possible	Partially possible
3	Frequency accuracy	Not accurate	Not accurate	Accurate	Accurate	Not accurate
4	Frequency and time resolution	Marginally good	Good	Better	Good	Frequency resolution average and time resolution high
5	Robustness	Poor	Good	Very good	Good	Medium
6	Performance for processing of nonstationary signal	Fail	Affected	Not affected	Marginally affected	Marginally affected

(ii) Statistical formulation is proposed to locate faults on the power transmission line. Faults are classified by the estimation of number of faulty phases. The involvement of ground during fault condition is identified by the use of a hybrid ground fault index (HGFI).

(iii) Protection scheme is effective to detect the fault events of SPGF, TPF, TPGF, TLF, and TLGF in a time duration of 0.0006 s. The algorithm successfully detected these faults in the conditions of fault impedance variation, variation in fault incidence angle, power flow on transmission line in the reverse direction, highly loaded line, different fault locations online, and noisy conditions.

(iv) Protection scheme is effective in locating the faults on a transmission line with a mean error of 0.968% and an average accuracy of 99.031%.

(v) Protection scheme is also effective to detect a fault on a practical transmission line of utility grid.

(vi) Protection scheme performs well compared with the protection schemes based on the use of HHT and WT in terms of mean error of fault location, fault location accuracy, and noise level.

(vii) Protection scheme is effective to recognize and discriminate fault events even when a noise of 10 dB SNR is present.

1.4. Outline of Paper. The research contents in the study are arranged in nine sections. The background of research and contribution is introduced in the first section. The transmission line used to perform the study is described in the second section. The proposed HSTLP is described in the third section. Simulation results to detect and categorize fault events are discussed in the fourth section. Simulation results to establish the performance of algorithm during various case studies are detailed in the fifth section. The fault location on transmission line is detailed in the sixth section. The validation of protection technique on a practical transmission line of an utility network is discussed in the seventh section. Performance is compared with reported algorithms in the eighth section. Research work is concluded in the ninth section of the study.

2. Transmission Line Test System

A two-terminal transmission line (TL) of length of 220 km is considered for the study, which is described in Figure 1. This transmission line is connected between complex networks of two utility grids. Generally, for every transmission line, which is a part of utility grid, there is a complex network on both ends. Hence, utility grid 1 (UG-1) and utility grid 2 (UG-2) considered in this study represent the real-time scenario of power grids. Bus 1 and bus 2 are considered for the termination of line at both ends. Circuit breakers (CBs) are installed on both sides of every bus to isolate during the fault condition. A current transformer (CT) is installed near bus 1 to capture the current. This current is continuously monitored and decomposed by the proposed hybrid protection scheme to generate a trip command for the CB-2 during the condition of faulty event for tripping the line. Technical parameters of the transmission line and utility grid are provided in Table 2 [19, 20].

3. Hybrid Transmission Line Protection Scheme

The proposed hybrid transmission line protection scheme is framed by the hybridization of features computed using the Stockwell transform (ST), Wigner distribution function (WDF), and alienation coefficient for the detection of faults. The hybrid ground fault index and number of faulty phases are used to discriminate different natures of faults. Statistical formulation is utilized for fault location. All steps of the proposed hybrid TL protection scheme are illustrated in Figure 2 and described in the below subsections.

3.1. Fault Detection. The hybrid signal processing fault index (HSPFI) is computed using the Stockwell transform (ST), WDF, and ACF as described in the following subsections.

3.1.1. Stockwell Fault Index. The Stockwell transform is developed by the evolution of wavelet transform (WT) to represent a signal in time-frequency form. This time-frequency representation gives higher frequency resolution than WT corresponding to all frequency spectra associated with the signal. The Gaussian function is utilized as a

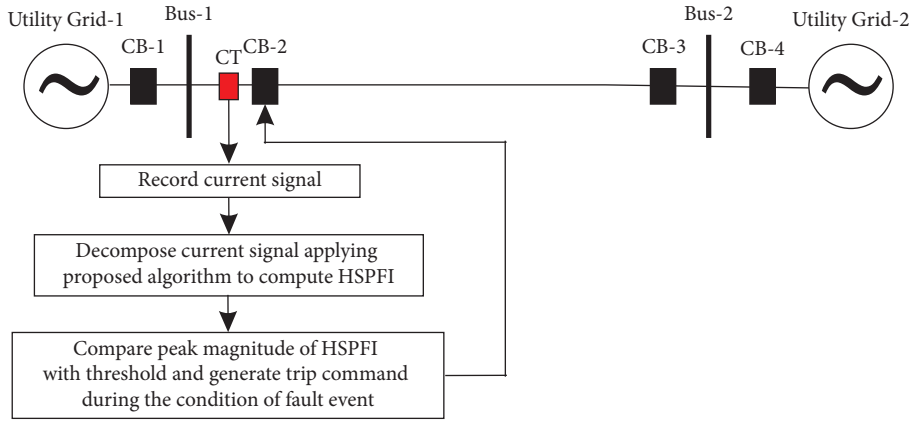

Figure 1: Two-terminal transmission line used for the study.

Table 2: Technical parameters of test network.

S. no.	Description of technical parameter	Magnitude of technical parameter
1	Length of transmission line	220 km
2	Voltage of UG-1	$500\angle 20^{\circ}$ kV
3	Equivalent impedance of UG-1	$17.117 + j45.529\Omega$
4	Voltage of UG-2	$500\angle^{0^{\circ}}$ kV
5	Equivalent impedance of UG-2	$15.31 + j45.529\,\Omega$
6	Positive sequence impedance of TL	$4.983 + j117.83\,\Omega$
7	Zero sequence impedance of TL	$12.682 + j264.196\,\Omega$
8	Positive sequence admittance of TL	$j1.468$ m$\mho$
9	Zero sequence admittance of TL	$j1.099$ m$\mho$
10	Apparent power capacity of TL	433.63 (MW) $+ j294.52$ (MVAR)

window for ST, and the length of this window is variable and inversely proportional to the magnitude of signal frequency. The Gaussian window is updated by multiplying a phase correction factor, which is an oscillatory exponential function [21]. The decomposition of a current signal ($i(t)$) using ST is expressed by the following mathematical formulation [22]:

$$S(\tau, f) = \int_{-\infty}^{\infty} i(t) g(\tau - t) e^{-2\pi f t}\, \mathrm{d}t, \tag{1}$$

where $g(\tau)$ is the Gaussian modulation function and is defined by the following mathematical formulation [22]:

$$g(\tau) = \frac{|f|}{\sqrt{2\pi}} e^{-\left(\tau^2/(2\sigma^2)\right)}, \tag{2}$$

where σ is defined as reciprocal of magnitude of frequency as detailed below [22]:

$$\sigma = \frac{1}{|f|}. \tag{3}$$

The output matrix of ST ($S(\tau, f)$) is used to compute the Stockwell fault index (SFI). The median ST index (MSTI) is computed by taking the median of every column of the matrix $S(\tau, f)$ as detailed below:

$$\mathrm{MSTI} = \mathrm{median}\,(S(\tau, f)). \tag{4}$$

The variance ST index (VSTI) is computed by taking the variance of every column of the matrix $S(\tau, f)$ as detailed below:

$$\mathrm{VSTI} = \mathrm{var}\,(S(\tau, f)). \tag{5}$$

The Stockwell fault index (SFI) is derived by the multiplication of MSTI and VSTI element to element as detailed below:

$$\mathrm{SFI} = \mathrm{MSTI} \times \mathrm{VSTI}. \tag{6}$$

3.1.2. Wigner Fault Index. The current signals are decomposed using the Wigner distribution function (WDF) using a sampling frequency equal to 3.84 kHz to compute the Wigner fault index (WFI). The window of samples over a quarter cycle is used to compute the WFI, which is moved forward by one sample each time. WDF used for fault identification uses energy density of current waveform in the time-frequency plane. The time-domain current ($I(t)$) is considered twice due to which it is taken as bilinear analysis. WDF provides merit of higher resolution for time-frequency and energy concentration to compute the WFI [23]. The WFI for the current signal ($I(t)$) is computed using the following mathematical formulation:

$$\mathrm{WFI} = \int_{-\infty}^{\infty} I\left(t + \frac{\tau}{2}\right) I^{*}\left(t + \frac{\tau}{2}\right) e^{-j\omega\tau}\, \mathrm{d}\tau, \tag{7}$$

where t: time, which is a sliding variable, ω: angular frequency of current signal, and τ: time-domain signal function.

3.1.3. Alienation Coefficient Fault Index. The sample-based ACF of current waveform (sampling frequency equal to 3.84 kHz) is utilized for computing the ACF-based fault index (ACFI). The correlation coefficient (CC) of quantities x and y is computed using the following relation [24]:

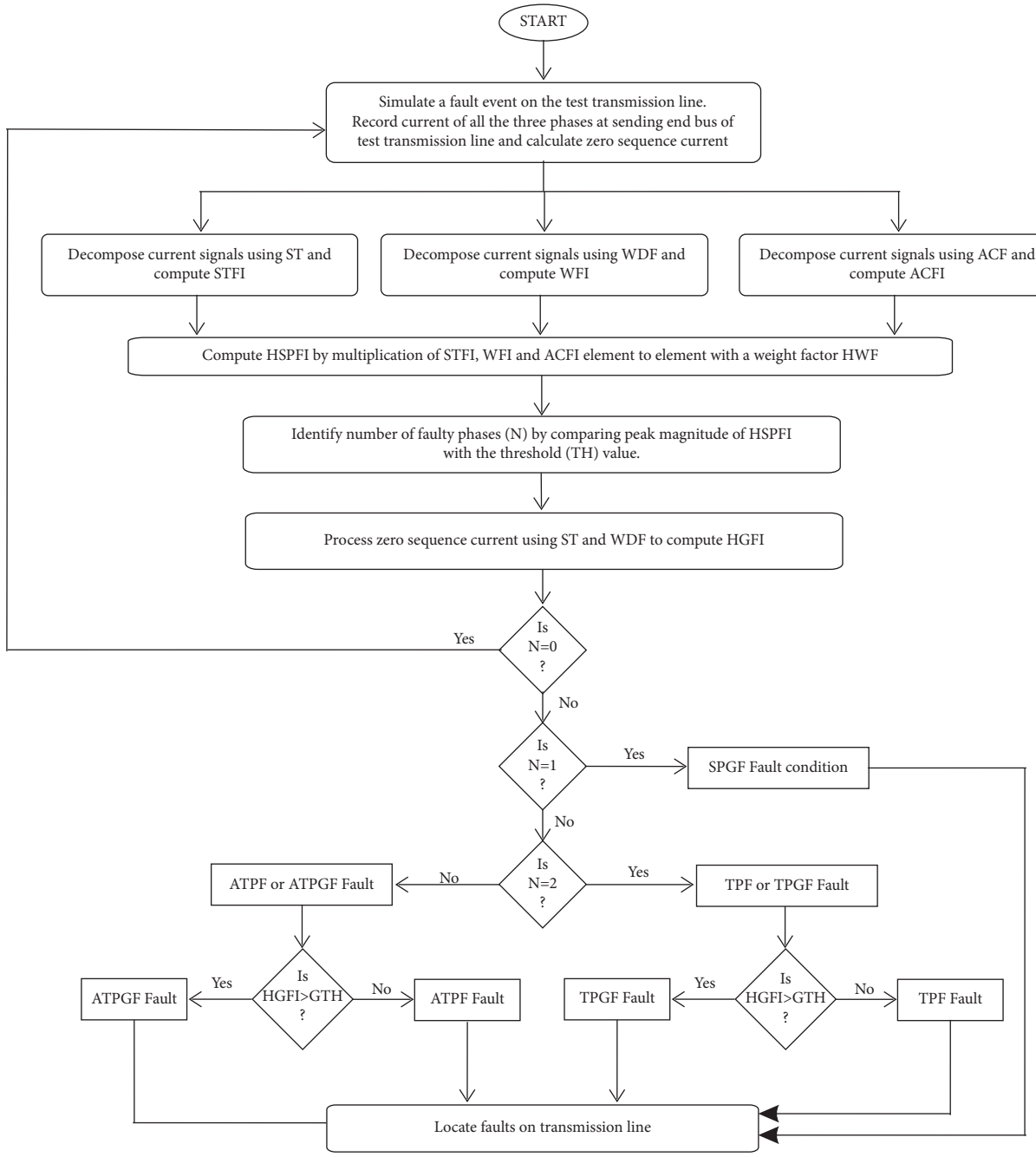

Figure 2: Hybrid transmission line protection scheme.

$$\mathrm{CC} = \frac{N_s \Sigma xy - (\Sigma x)(\Sigma y)}{\sqrt{\left[N_s \Sigma x^2 - (\Sigma x)^2\right]\left[N_s \Sigma y^2 - (\Sigma y)^2\right]}}, \tag{8}$$

where symbols are defined as follows: N_s: sample number in a cycle of current signal (64 samples are used in this study), x: current samples measured at initial time t_0, y: current samples measured at time $-T + t_0$, and T: time period of current signal. The moving window utilized for the computation of CC is illustrated in Figure 3. Here, the quarter cycle window is used to compare the current samples of a quarter cycle with already recorded data of the previous healthy cycle of current signal. Hence, any deviation from the healthy nature of cycle during faulty event will be recognized.

The alienation coefficient-based fault index is derived from CC as per the following relation:

$$\mathrm{ACF} = 1 - \mathrm{CC}^2. \tag{9}$$

3.1.4. Hybrid Signal Processing Fault Index. The hybrid signal processing fault index (HSPFI) is derived by multiplying the SFI, WFI, and ACFI element to element as detailed below:

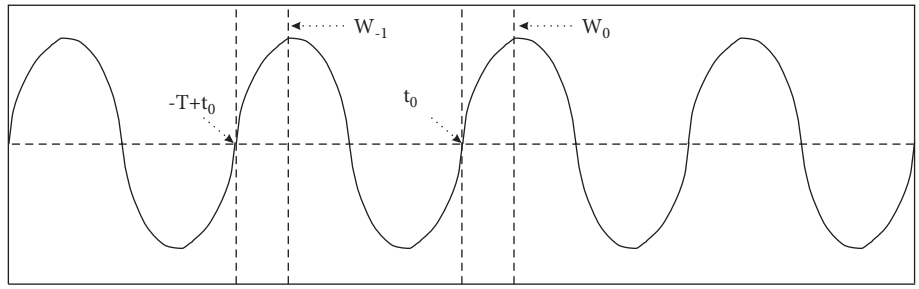

Figure 3: Computation of ACFI.

$$\text{HSPFI} = \text{SFI} \times \text{WFI} \times \text{ACFI} \times \text{HWF}, \quad (10)$$

where HWF is the hybrid weight factor used to make the magnitude of HSPFI significantly high so that faulty events may be detected and discriminated with high resolution and accuracy. In this study, HWF is considered equal to 50. A threshold magnitude (TH) of 5000 is considered to detect the faulty conditions and differentiate these events from the healthy condition of the transmission line. The magnitude of TH equal to 5000 is decided after testing the algorithm for 32 data sets of each type of fault considering the different case studies such as fault impedance variations, variations in fault location on transmission line, different noise levels, variations in fault incidence angle, reverse power flow, different line loading, and various sampling frequencies.

3.2. Hybrid Ground Fault Index. A hybrid ground fault index (HGFI) is designed to detect ground involvement during a faulty event. This is used to discriminate the TPF from the TPGF. Similarly, this is also used to discriminate the TLF from the TLGF events. HGFI is derived by decomposing zero sequence current (I_0). Zero sequence current is calculated from currents associated with all the three phases (I_a, I_b, and I_c) by taking the average magnitude as detailed below:

$$I_0 = \frac{I_a + I_b + I_c}{3}. \quad (11)$$

Zero sequence current (I_0) is analyzed using the mathematical tool described in Section 3.1.1, and the Stockwell ground fault index (SGFI) is computed. Further, zero sequence current is also decomposed using the mathematical tool elaborated in Section 3.1.2 to compute the Wigner ground fault index (WGFI). The SGFI and WGFI are multiplied to derive the hybrid ground fault index.

$$\text{HGFI} = \text{SGFI} \times \text{WGFI}. \quad (12)$$

A ground threshold value (GTH) equal to 50 is considered to recognize the ground involvement during a fault event. The peak magnitude of HGFI is greater than the threshold value when ground is involved during the fault event. Alternatively, when ground is not participated during a fault event then the magnitude of HGFI is nearly zero.

3.3. Location of Fault Events. The location of fault events on the transmission line is determined using statistical formulations designed using the curve fitting method based on the standard deviation of the HSPFI. The following mathematical formulation is proposed for locating faulty condition on transmission line:

$$l = ax^b, \quad (13)$$

where l = line length from sending terminal bus of the transmission line; a and b are coefficients and are dependent on the type of fault event and the magnitude of these coefficients used to locate various fault events is provided in Table 3. The formulation for fault location is designed with root-mean-square error (RMSE) equal to 8.12 and squared estimate of errors (SSE) equal to 593.4.

Table 3: Magnitude of coefficients used for fault location.

S. no.	Type of fault event	Magnitude of coefficient	
		a	b
1	SPGF	1692	−0.3761
2	TPF	1935	−0.3167
3	TPGF	2130	−0.3257
4	TLGF	5033	−0.3975

4. Simulation Results: Identification of Faults

The identification of fault events including SPGF, TPF, TPGF, TLF, and TLGF using the proposed algorithm is discussed in this section. Further, the categorization of fault events is also discussed in this section.

4.1. Single-Phase-to-Ground Fault. A SPGF is simulated at the middle (at line length of 110 km from bus 1) of transmission line on phase A, and current signals are recorded at bus 1, which are illustrated in Figure 4(a). These currents are processed using ST, and SFI is computed, which is described in Figure 4(b). Currents are processed by applying WDF, and WFI is computed, which is shown in Figure 4(c). Further, currents are also processed by applying the alienation coefficient, and ACFI is computed, which is described in Figure 4(d). HSPFI is computed by the multiplication of SFI, WFI, ACFI, and hybrid weight factor (HWF), which is described in Figure 4(e). A high-resolution curve of HSPFI is described in Figure 4(f).

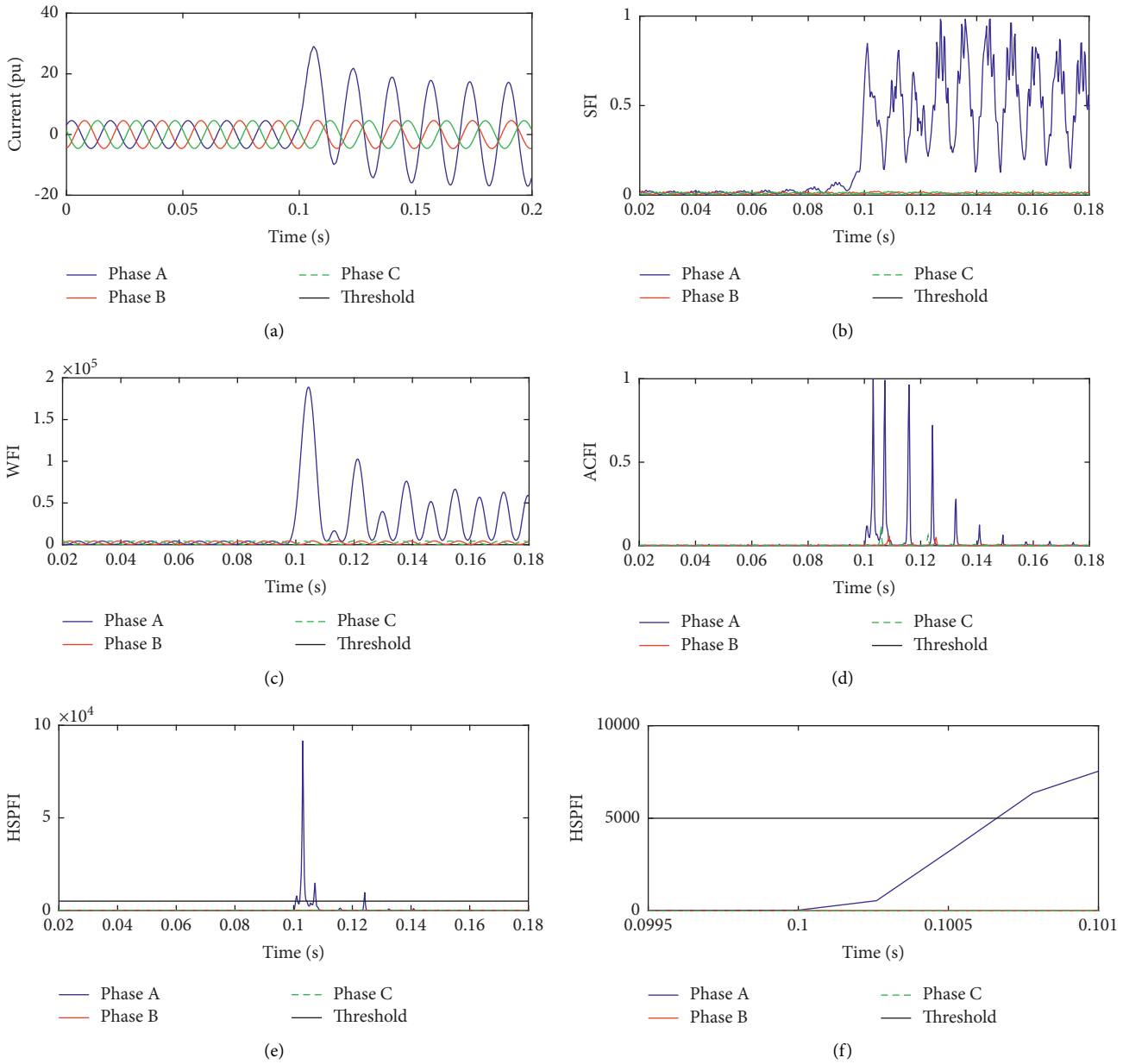

Figure 4: SPGF: (a) current waveform, (b) SFI, (c) WFI, (d) ACFI, (e) HSPFI, and (f) high-resolution cure of HSPFI.

Figure 4(a) described that current of faulty phase is increased due to SPGF on phase A at 0.1 s and there is no significant change in the current of healthy phases A and B. Figure 4(b) details that the magnitude of SFI of faulty phase A has increased due to SPGF and the magnitude of SFI for healthy phases is nearly zero. Figure 4(c) elaborates that the magnitude of WFI for faulty phase A has increased due to the occurrence of fault and this magnitude remains near zero for the healthy phase. Figure 4(d) illustrates that peaks of unit magnitude are associated with the ACFI plot of faulty phase A and ACFI is near zero for healthy phases. Figure 4(e) indicates that the magnitude of HSPFI for faulty phase A has crossed the threshold (TH) just after the fault incidence. However, due to the occurrence of fault event, the magnitude of HSPFI for healthy phases is below the threshold. Hence, the SPGF event is recognized effectively by the application of HSPFI. It is inferred from the high-resolution curve of HSPFI described in Figure 4(f) that the SPGF event is recognized in a time duration of 0.0006 s.

4.2. Two-Phase Fault. A two-phase fault (TPF) is simulated at the middle (at line length of 110 km from bus 1) of transmission line on phases A and B. Currents are recorded at bus 1, which are illustrated in Figure 5(a). These currents are processed using ST for computing SFI, which is described in Figure 5(b). Currents are also processed using WDF to compute WFI, which is shown in Figure 5(c). Further, currents are processed using the alienation coefficient to compute ACFI, which is described in Figure 5(d). HSPFI is computed

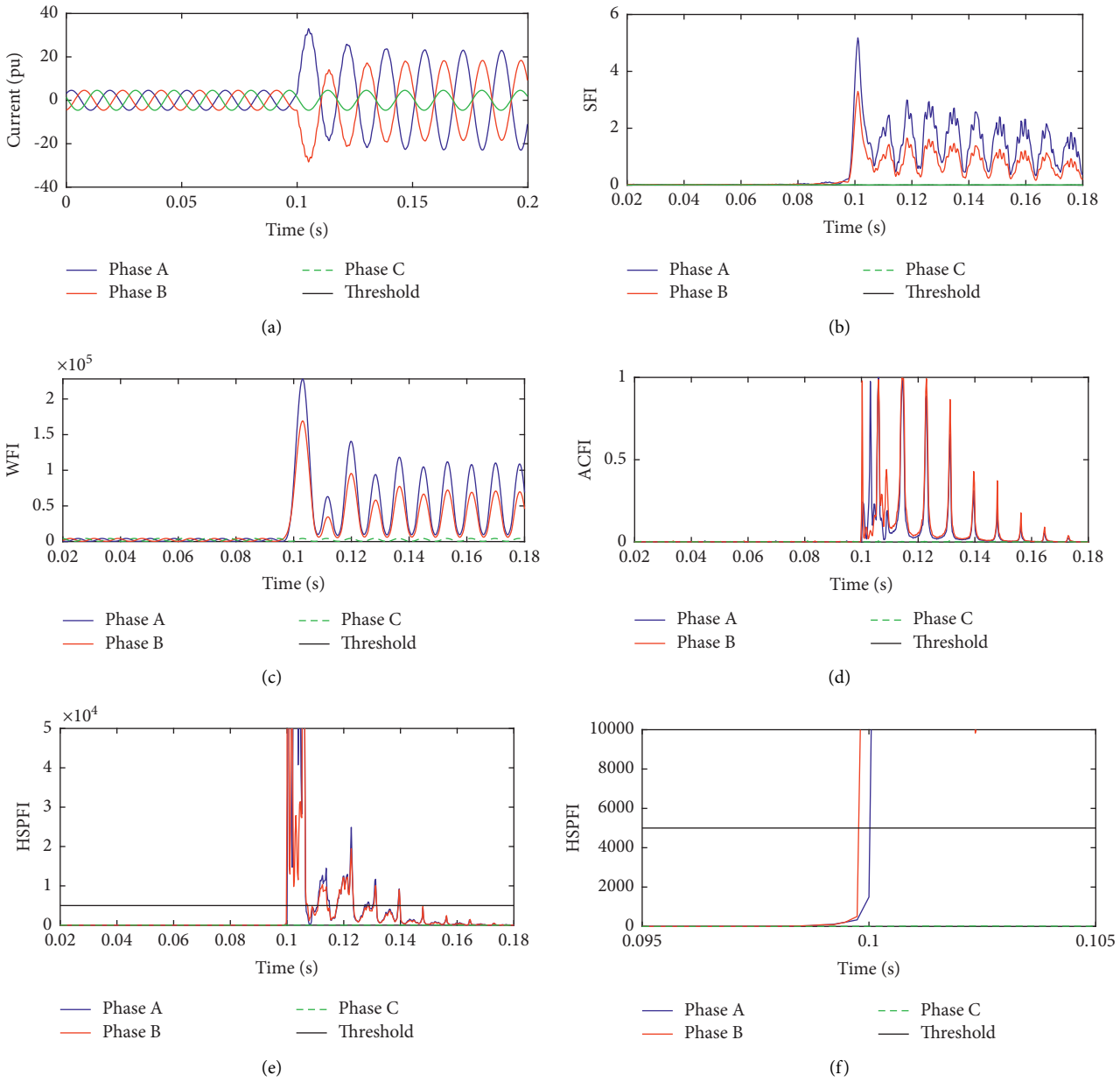

Figure 5: Two-phase fault: (a) current signals, (b) SFI, (c) WFI, (d) ACFI, (e) HSPFI, and (f) high-resolution curve of HSPFI.

by the multiplication of SFI, WFI, ACFI, and hybrid weight factor (HWF), which is described in Figure 5(e). A high-resolution curve of HSPFI is illustrated in Figure 5(f).

Figure 5(a) indicates that currents of faulty phases A and B have increased due to the occurrence of TPF on phases A and B at 0.1 s and there is no significant change in the current associated with the healthy phase C. Figure 5(b) illustrates that magnitudes of SFI for faulty phases A and B have increased due to the occurrence of TPF and magnitude of SFI for healthy phase C is nearly zero. Figure 5(c) elaborates that magnitudes of WFI for faulty phases A and B have increased due to the occurrence of fault and this magnitude for healthy phase C remains nearly zero. Figure 5(d) illustrates that peaks of unit magnitude are associated with the ACFI plot of faulty phases A and B and ACFI remains near zero for the healthy phase C. Figure 5(e) details that magnitudes of HSPFI for faulty phases A and B have crossed the threshold (TH) just after the fault incidence. However, due to the occurrence of fault event, the magnitude of HSPFI for healthy phase C is below the threshold. Hence, TPF is identified effectively by the use of HSPFI. It is inferred from the high-resolution plot of HSPFI described in Figure 5(f) that TPF event is detected in a time duration of 0.0002 s.

4.3. Two-Phase-to-Ground Fault. A two-phase-to-ground fault (TPGF) is realized at central location (at line length of 110 km from bus 1) of transmission line on phases A and B. Currents are recorded at bus 1, which are illustrated in

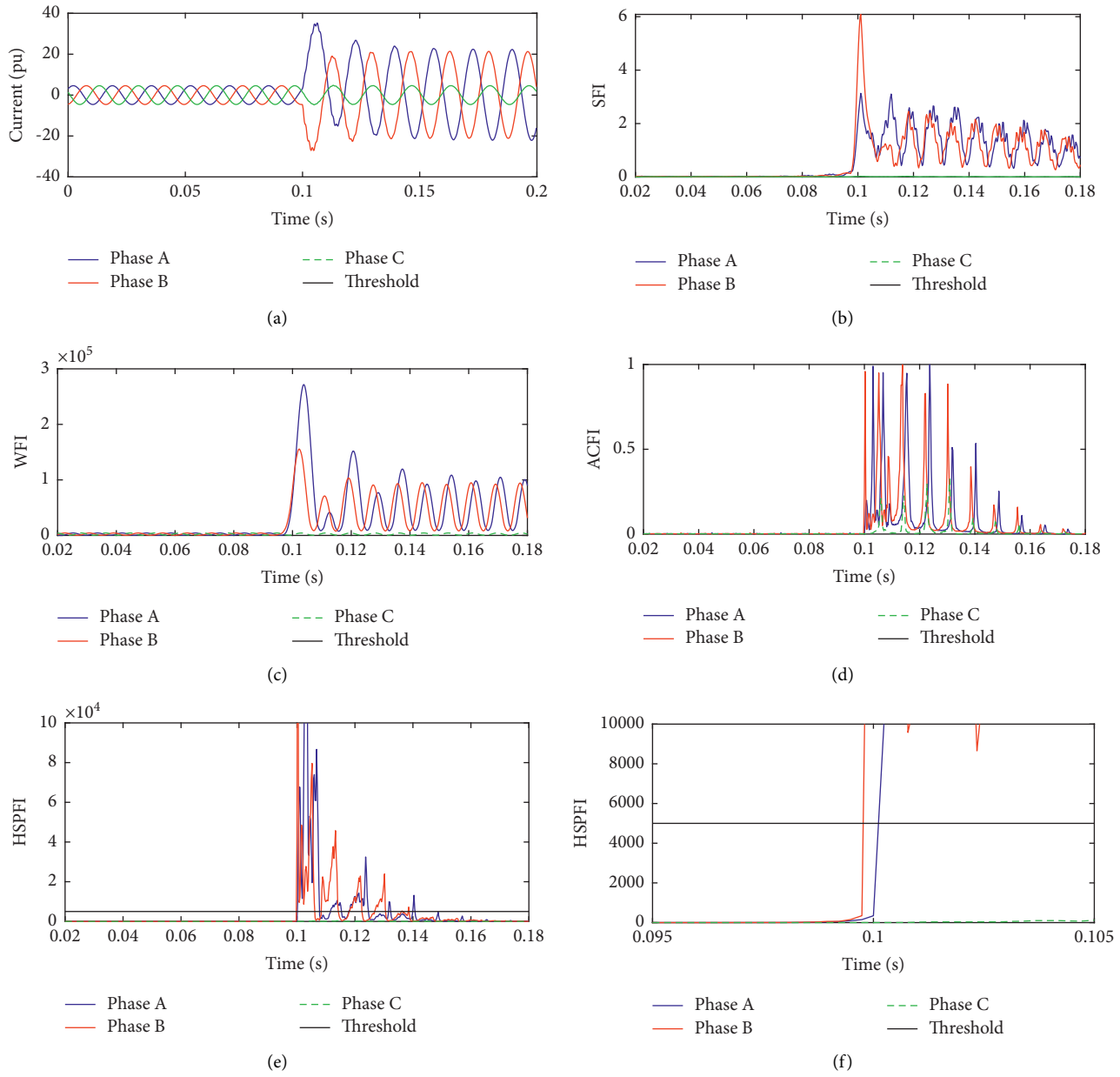

Figure 6: Two-phase-to-ground fault: (a) current waveform, (b) SFI, (c) WFI, (d) ACFI, (e) HSPFI, and (f) high-resolution plot of HSPFI.

Figure 6(a). These currents are processed using ST for computing SFI, which is described in Figure 6(b). Currents are also processed using WDF for computing WFI, which is shown in Figure 6(c). Further, currents are processed using the alienation coefficient to compute ACFI, which is described in Figure 6(d). HSPFI is computed by the multiplication of SFI, WFI, ACFI, and hybrid weight factor (HWF), which is described in Figure 6(e). A high-resolution curve of HSPFI is described in Figure 6(f).

Figure 6(a) indicates that currents of faulty phases A and B have increased due to the occurrence of TPGF on phases A and B at 0.1 *s* and there is no significant change in the current associated with the healthy phase C. Figure 6(b) illustrates that magnitudes of SFI for faulty phases A and B have increased due to the occurrence of TPGF and magnitude of this index for healthy phase C is nearly zero. Figure 6(c) elaborates that magnitudes of WFI for faulty phases A and B have increased due to the occurrence of fault and this magnitude for healthy phase C remains nearly zero. Figure 6(d) illustrates that peaks of unit magnitude are associated with the ACFI plot of faulty phases A and B and ACFI remains near zero for the healthy phase C. Figure 6(e) indicates that magnitudes of HSPFI for faulty phases A and B have crossed the threshold (TH) just after fault incidence. However, due to the occurrence of fault the magnitude of HSPFI for healthy phase C is below the threshold. Hence, TPGF is identified effectively by the application of HSPFI. It is inferred from the high-resolution curve of HSPFI described in Figure 6(f) that the TPGF event has been detected in a time duration of 0.0002 *s*.

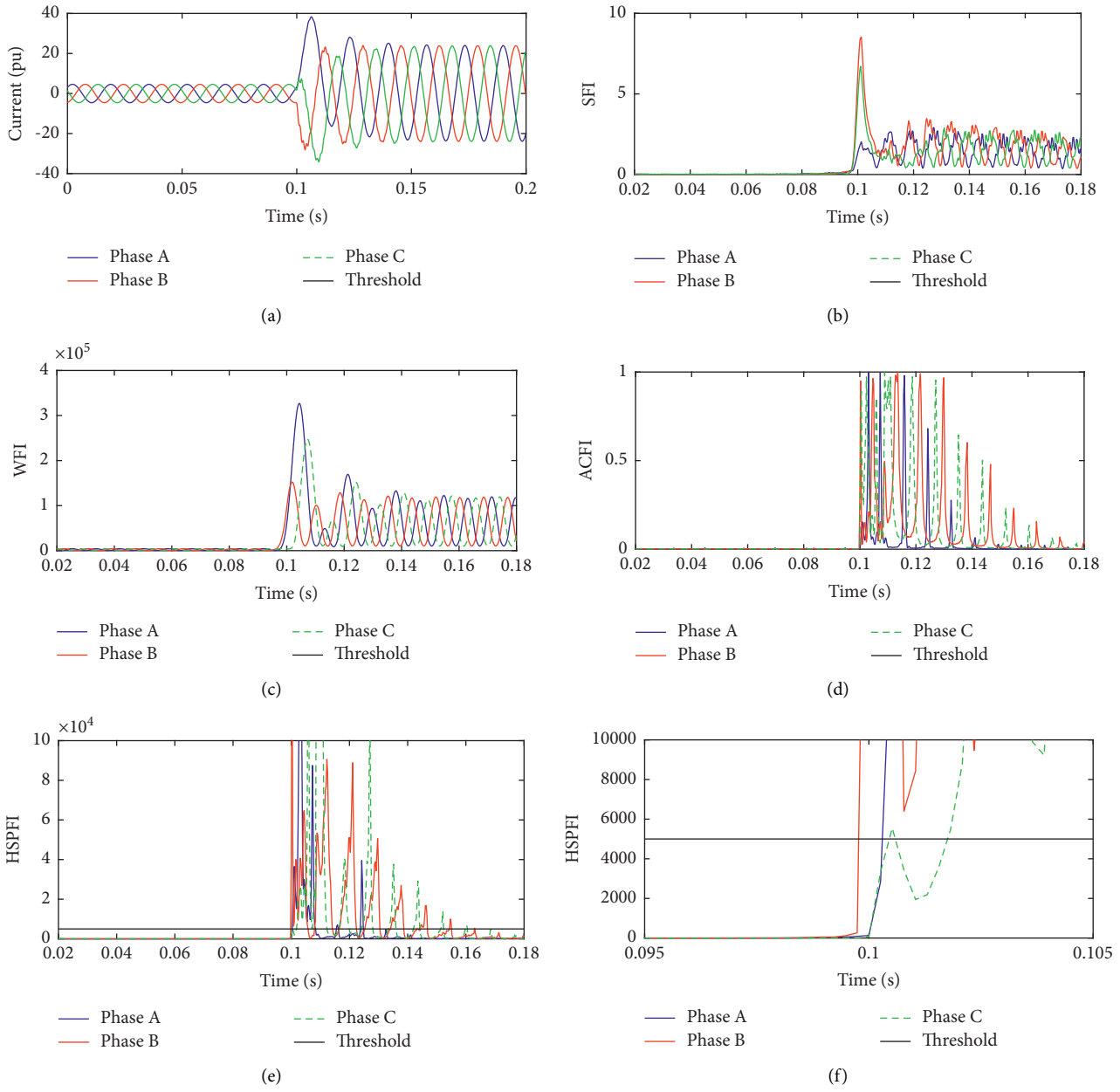

Figure 7: Three-line fault: (a) currents, (b) SFI, (c) WFI, (d) ACFI, (e) HSPFI, and (f) high-resolution plot of HSPFI.

4.4. Three-Line Fault. A three-line fault (TLF) without the involvement of ground is simulated at the middle (at line length of 110 km from bus 1) of test transmission line. Currents are recorded at bus 1, which are illustrated in Figure 7(a). These currents are processed using ST to compute SFI, which is described in Figure 7(b). Currents are also processed using WDF for computing WFI, which is shown in Figure 7(c). Further, currents are processed using the alienation coefficient for computing ACFI, which is described in Figure 7(d). HSPFI is computed by the multiplication of SFI, WFI, ACFI, and hybrid weight factor (HWF), which is described in Figure 7(e). A high-resolution curve of HSPFI is shown in Figure 7(f).

Figure 7(a) indicates that currents of all phases have increased due to the occurrence of TLF at 0.1 *s*. Figure 7(b) illustrates that magnitudes of SFI for all the phases have increased due to the occurrence of TLF and the magnitude of healthy phase C is nearly zero. Figure 7(c) elaborates that magnitudes of WFI associated with all the phases have increased due to the incidence of fault. Figure 7(d) illustrates that peaks of unit magnitude are associated with ACFI plot of all the phases. Figure 7(e) describes that magnitudes of HSPFI associated with all the phases have crossed the threshold (TH) just after the fault incidence. Hence, TLF event is identified effectively by the application of HSPFI. It is inferred from the high-resolution plot of HSPFI described in Figure 7(f) that TLF event has been detected in a time interval of 0.0003 *s*.

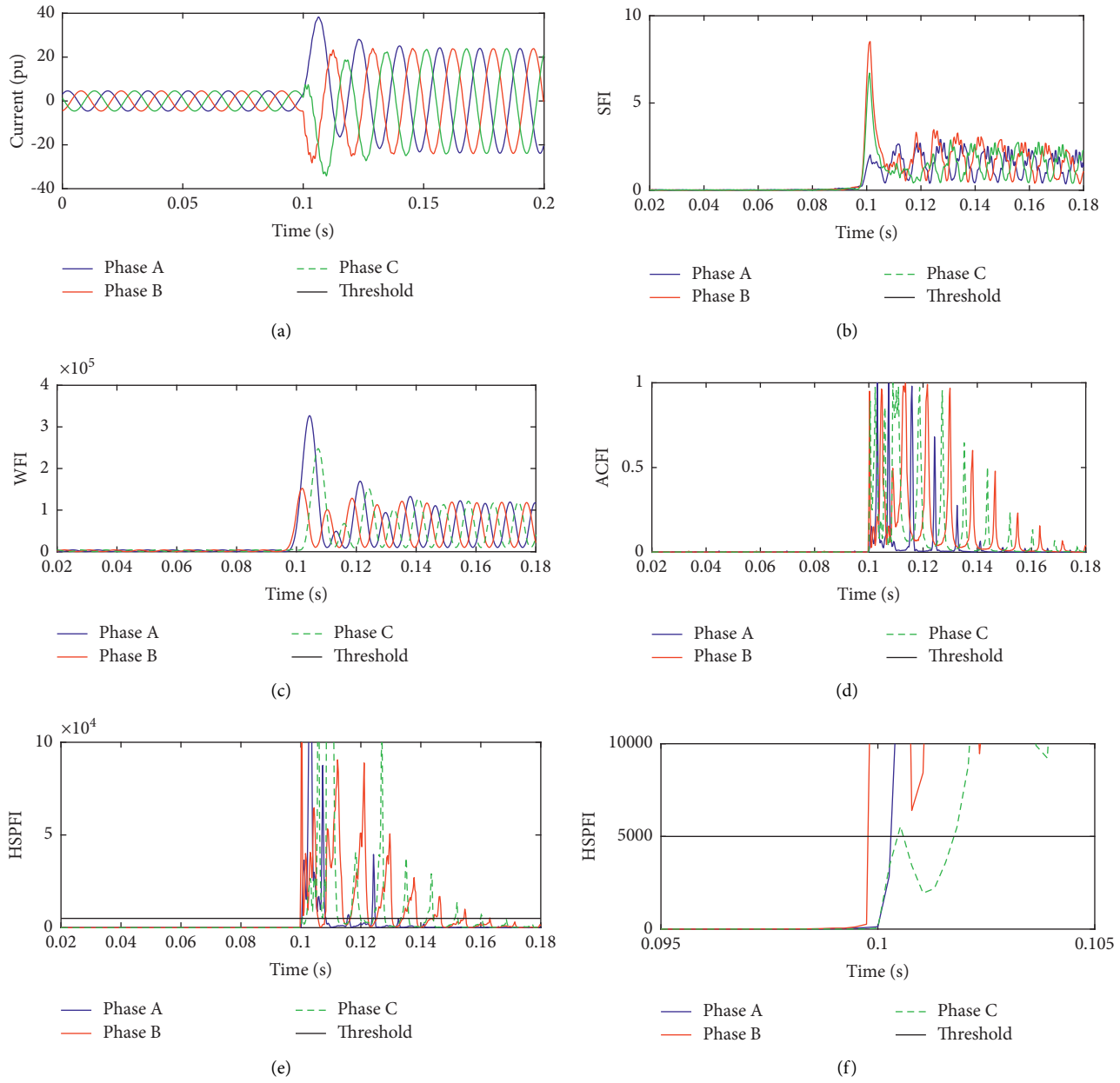

Figure 8: Three-line-to-ground fault: (a) current waveform, (b) SFI, (c) WFI, (d) ACFI, (e) HSPFI, and (f) high-resolution plot of HSPFI.

4.5. Three-Line-to-Ground Fault. A fault on all three lines and ground (TLGF) is simulated at the middle (at line length of 110 km from bus 1) of test transmission line. Current signals of all three phases are recorded at bus 1, which are illustrated in Figure 8(a). These currents are processed using ST for computing SFI, which is described in Figure 8(b). Currents are also processed using WDF for computing WFI, which is shown in Figure 8(c). Further, currents are processed using the alienation coefficient for computing ACFI, which is described in Figure 8(d). HSPFI is computed by the multiplication of SFI, WFI, ACFI, and hybrid weight factor (HWF), which is described in Figure 8(e). A high-resolution curve of HSPFI is described in Figure 8(f).

Figure 8(a) indicates that currents of all phases have increased due to the occurrence of TLGF at 0.1 s. Figure 8(b) illustrates that magnitudes of SFI for all the phases have increased due to the occurrence of TLGF and the magnitude of this index for healthy phase C is nearly zero. Figure 8(c) elaborates that magnitudes of WFI associated with all the phases have increased due to the occurrence of fault. Figure 8(d) illustrates that peaks of unit magnitude are associated with the ACFI plot of all the phases. Figure 8(e) describes that magnitudes of HSPFI associated with all the phases have crossed the threshold (TH) just after the fault incidence. Hence, TLGF is recognized effectively by the application of HSPFI. It is inferred from the high-resolution curve of HSPFI described

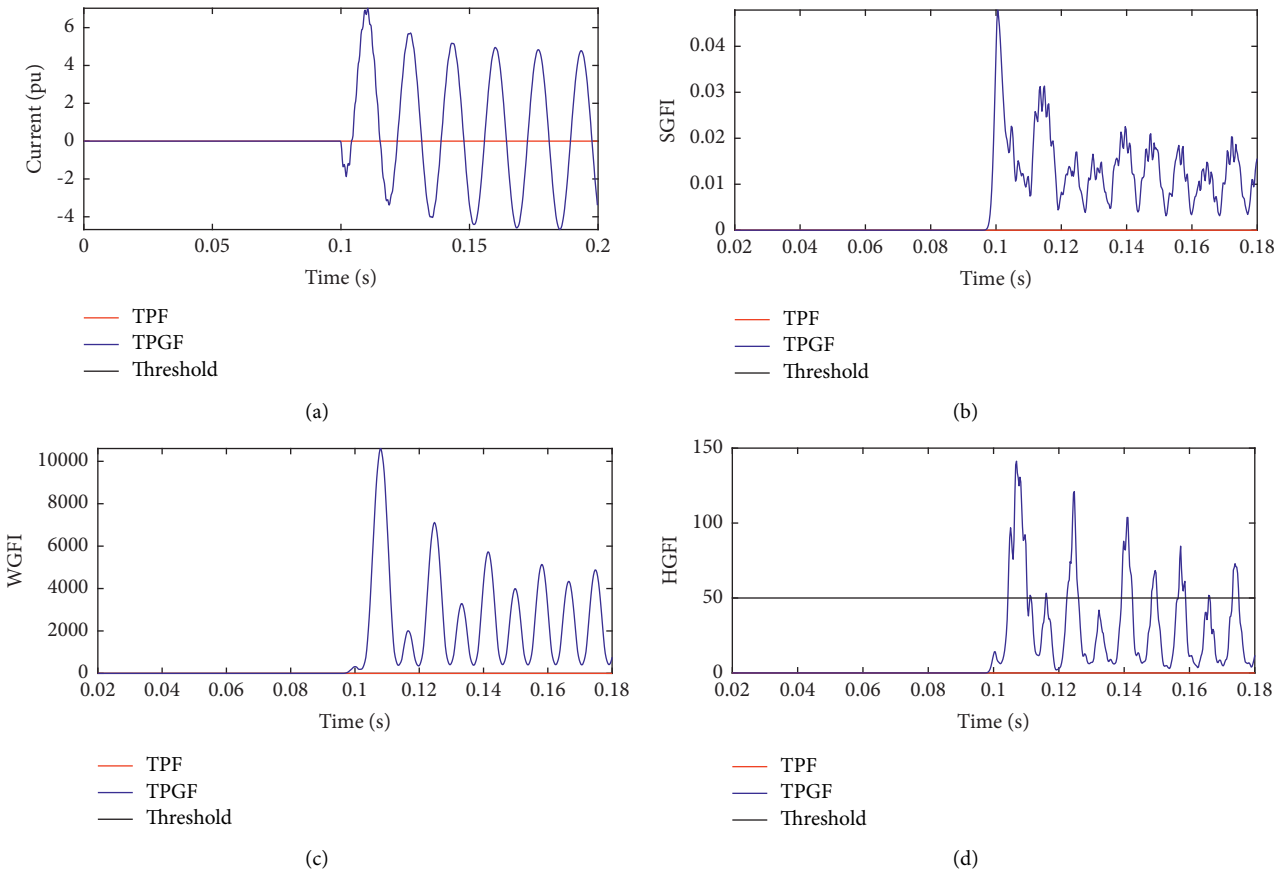

Figure 9: HGFI for discrimination of TPF and TPGF: (a) zero sequence current, (b) SGFI, (c) WGFI, and (d) HGFI.

in Figure 8(f) that TLF event is detected in a time duration of 0.0003 s.

4.6. Categorization of Fault Events. Fault types have been identified by the categorization of all faults in different categories. This is achieved by estimating the number of faulty phases by comparison of maximum magnitude of HSPFI with a preset threshold (TH). If the maximum magnitude of HSPFI is greater than TH for one phase only, then fault is SPGF. When the maximum magnitude of HSPFI is greater than TH for two phases, then fault is either TPF or TPGF. During conditions of TLF and TLGF, the magnitude of HSPFI is higher than TH for all phases. A HGFI computed by processing the zero sequence current is used to discriminate the TPF and TPGF as illustrated in Figure 9. Zero sequence currents are processed using ST to compute the Stockwell ground fault index (SGFI). Zero sequence currents are processed using WDF to compute the Wigner ground fault index (WGFI). SGFI and WGFI are multiplied to compute the hybrid ground fault index (HGFI). A ground threshold (GTH) equal to 20 is decided to detect ground involvement during the fault event. The magnitude of HGFI is greater than ground threshold when ground is involved during TPGF event. Figure 9(a) depicts that during the TPF event zero sequence current is zero, whereas it is nonzero after the occurrence of TPGF event. Figure 9(b) shows that magnitude of SGFI is increased due to the incidence of TPGF event and remains zero after the occurrence of TPF event. Similarly, the magnitude of WGFI is increased due to the incidence of TPGF and remains zero after the occurrence of TPF. Figure 9(d) illustrates that the magnitude of HGFI is increased and crossed the GTH due to the incidence of TPGF, whereas the magnitude of HGFI remains zero after the incidence of TPF. Hence, TPGF and TPF events have been discriminated from each other by the use of HGFI. Similarly, the HGFI is also effective to discriminate the TLF and TLGF events from each other.

5. Simulation Results: Case Studies

Simulation results of various cases of study are discussed in this section.

5.1. Effect of Variations in Fault Incidence Angle. A SPGF is simulated at the middle (at line length of 110 km from bus 1) of transmission line on phase A with the angle of fault incidence equal to 0°, 30°, 45°, 60°, 90°, 120°, 135°, 150°, and 180°. Currents are recorded at bus 1 and processed by the application of designed algorithm to compute HSPFI for all fault incidence angles. The peak magnitude of HSPFI for all three phases for different fault incidence angles is provided in Table 4. It is observed that the peak magnitude of HSPFI

Table 4: Effect of variations in angle of fault incidence.

Bus no.	Angle of fault incidence	Maximum value of HSPFI		
		Phase A	Phase B	Phase C
1	0°	**91524**	108.44	119.74
2	30°	2.5691×10^5	251.93	138.67
3	45°	2.9595×10^5	675.73	477.63
4	60°	1.6308×10^5	266.15	1373.3
5	90°	**93378**	953.85	882.87
6	120°	**73084**	333.88	208.94
7	135°	**97760**	178.54	208.97
8	150°	1.0291×10^5	166.48	104.64
9	180°	**83280**	110.79	121.95

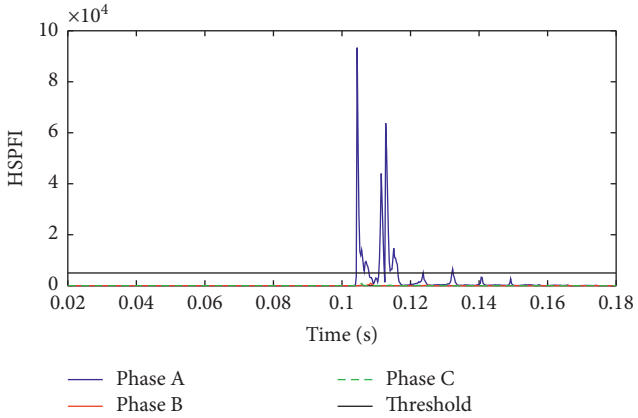

Figure 10: HSPFI for SPGF with 90° fault incidence angle.

for faulty phase A is higher than the threshold, whereas it is lower than the threshold for healthy phases A and B.

The HSPFI for fault incidence angle equal to 90° with the condition of SPGF event is detailed in Figure 10. It is inferred that after the incidence of SPGF event, the HSPFI associated with faulty phase A is higher relative to the threshold magnitude, whereas HSPFI for healthy phases A and B is lower than the threshold. Hence, the SPGF event is detected effectively considering the various fault incidence angles.

5.2. Effect of Location of Faults. A SPGF is simulated at various locations (10 km, 40 km, 80 km, 110 km, 150 km, 180 km, and 210 km) of transmission line on phase A. Currents of all the three phases are recorded at bus 1 and processed by the application of designed algorithm to compute HSPFI for all locations. The peak magnitude of HSPFI for all the three phases for various fault locations is provided in Table 5. It is inferred that the peak magnitude of HSPFI for faulty phase A is higher than the threshold, whereas it is lower than the threshold for healthy phases B and C. Hence, the SPGF has been effectively identified at various fault locations on transmission line.

5.3. Effect of Noise. A SPGF is simulated at the middle (at line length of 110 km from bus 1) of transmission line on phase A, and currents are recorded at bus 1. The Gaussian noise of 10 dB SNR (signal-to-noise ratio) is superimposed on current

Table 5: Effect of location of fault on transmission line.

Bus no.	Location of fault (line length from sending terminal in km)	Maximum value of HSPFI		
		Phase A	Phase B	Phase C
1	10	2.1821×10^6	3452.2	1804.6
2	40	1.0558×10^6	1905.3	1036.8
3	80	2.8789×10^5	388.99	383.39
4	110	**91524**	108.44	119.74
5	150	**38052**	116.35	136.71
6	180	**19699**	32.384	275.07
7	210	**17428**	76.121	498.37

waveform. Noisy currents are described in Figure 11(a). These currents with noise are processed using ST for computing SFI, which is described in Figure 11(b). Currents with noise are processed using the WDF to compute WFI, which is shown in Figure 11(c). Further, current signals with noise are also processed by the application of ACF to compute ACFI, which is detailed in Figure 11(d). HSPFI is computed by the multiplication of SFI, WFI, ACFI, and hybrid weight factor (HWF), which is described in Figure 11(e). A high-resolution curve of HSPFI is described in Figure 11(f).

Figure 11(a) indicates that noisy current of faulty phase has increased due to the incidence of SPGF event on phase A at 0.1 s and there is no significant change in the current of healthy phases A and B. Figure 11(b) indicates that the magnitude of SFI of faulty phase A has increased due to the occurrence of SPGF and magnitude of healthy phases is nearly zero. Figure 11(c) elaborates that magnitude of WFI of faulty phase A has increased due to the occurrence of fault and this magnitude associated with healthy phases remains nearly zero. Figure 11(d) illustrates that peaks of unit magnitude are associated with the ACFI plot of all phases before and after the incidence of fault on phase A. Hence, the performance of ACFI is adversely affected by the availability of noise. Figure 11(e) indicates that the magnitude of HSPFI for faulty phase A has crossed the threshold (TH) just after the fault incidence in noisy scenario. However, due to the incidence of fault event in the presence of noise the magnitude of HSPFI for healthy phases is lower than the threshold. Hence, the SPGF is identified effectively by the application of HSPFI in the availability of noise. It is inferred from the high-resolution plot of HSPFI described in Figure 11(f) that the SPGF event has been detected in a time duration of 0.0006 s.

5.4. Effect of Variation in Fault Impedance. A SPGF is realized at the middle (at line length of 110 km from bus 1) of transmission line on phase A considering the fault impedance of 0.01 Ω, 1 Ω, 2 Ω, 5 Ω, 10 Ω, 20 Ω, and 50 Ω. Currents of all phases are recorded at bus 1 and processed by the application of designed algorithm for computing HSPFI for all locations. The peak magnitude of HSPFI for all the three phases for various fault locations is provided in Table 6. It is observed that the maximum magnitude of HSPFI for faulty phase A is higher than the threshold, whereas it is lower than the threshold for healthy phases B and C. Hence, the SPGF is effectively identified for different magnitudes of fault impedance.

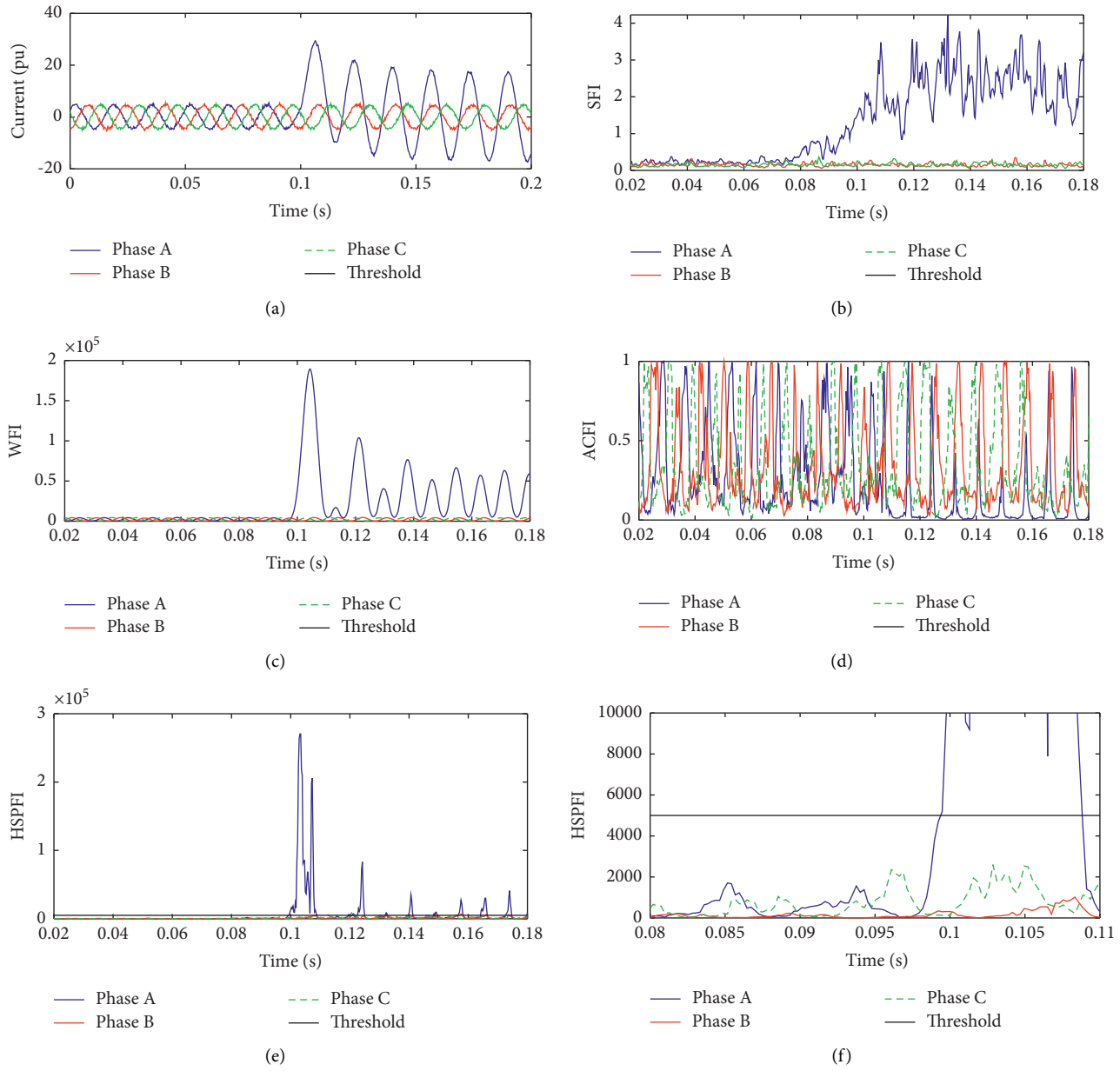

Figure 11: Effect of noise for the detection of SPGF on transmission line: (a) current signals, (b) SFI, (c) WFI, (d) ACFI, (e) HSPFI, and (f) high-resolution curve of HSPFI.

Table 6: Effect of fault impedance variation.

Bus no.	Fault impedance (Ω)	Maximum value of HSPFI		
		Phase A	Phase B	Phase C
1	0.01 Ω	**91524**	108.44	119.74
2	1 Ω	**87865**	109.18	119.55
3	2 Ω	**84626**	109.76	119.11
4	5 Ω	**75512**	110.45	116.81
5	10 Ω	**62559**	109.69	110.85
6	20 Ω	**43012**	101.49	93.366
7	50 Ω	**15853**	61.378	47.324

5.5. Effect of Reverse Power Flow. The direction of power flow on the test transmission line is reversed by changing phase angle of the generators used to design utility grid 1 and utility grid 2. A SPGF is simulated at the middle (at line length of 110 km from bus 1) of transmission line on phase A, and currents of all phases are recorded at bus 1. These current signals are processed to compute the HSPFI, which is illustrated in Figure 12. It is observed that HSPFI for faulty phase A is increased and becomes higher than the threshold magnitude due to the incidence of SPGF. The magnitude of HSPFI associated with the healthy phases is lower relative to the threshold. Hence, the SPGF event has been identified effectively during the condition of reverse power flow on transmission line.

5.6. Effect of Line Loading. An additional load of 200 MW is connected on receiving terminal bus 2 of test transmission

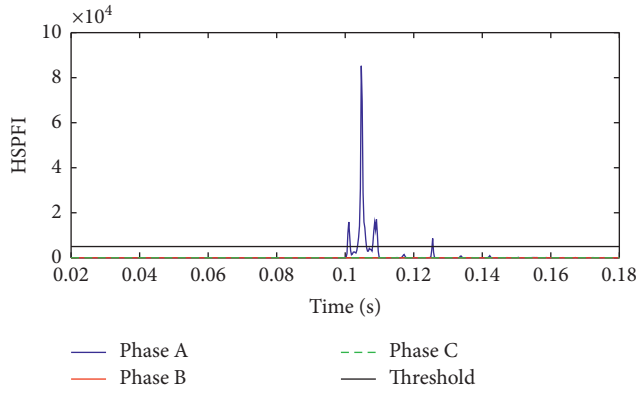

Figure 12: HSPFI indicating the effect of reverse power flow.

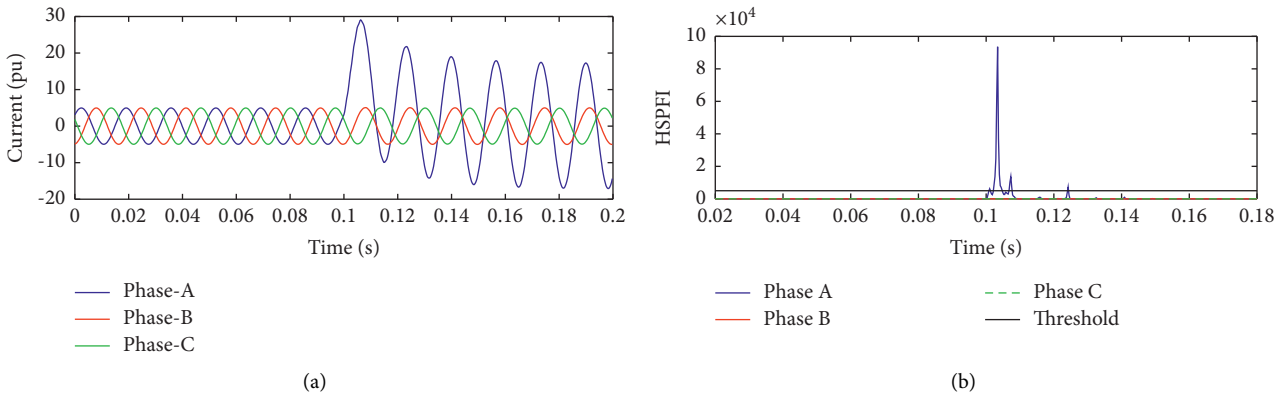

Figure 13: Effect of line loading: (a) current signal and (b) HSPFI.

line. A SPGF is simulated at the middle (at line length of 110 km from bus 1) of the transmission line on phase A, and currents of all phases are recorded at bus 1. Currents are described in Figure 13(a). It is indicated that currents of faulty phase A have increased just after the occurrence of fault and current of healthy phases A and B remains almost unchanged. The current signals are processed to compute the HSPFI, which is detailed in Figure 13(b). It is indicated that the magnitude of HSPFI for faulty phase A is increased and becomes higher than the threshold due to the occurrence of SPGF. The magnitude of HSPFI for healthy phases is lower than the threshold. Hence, the SPGF is identified effectively during the condition of loading on the transmission line.

5.7. Effect of Sampling Frequency. The performance of the designed protection algorithm is tested considering sampling frequencies of 1.28, 1.92, 3.84, 7.68, and 11.52 kHz. This is observed that the performance of protection algorithm considering sampling frequency below 3.84 kHz has increased the detection time and the performance is deteriorated with false tripping commands. Further, considering sampling frequency above 3.84 kHz has not improved the performance significantly in terms of accuracy and protection speed. Therefore, 3.84 kHz sampling frequency is considered as the optimal sampling frequency at which the performance of protection scheme is better and fast.

6. Location of Faults on Transmission Line

Faulty events are located on transmission line using the methodology detailed in Section 3.3. The standard deviation feature of the HSPFI for all the investigated fault events located at lengths of 10 km, 20 km, 30 km, 40 km, 50 km, 60 km, 70 km, 80 km, 90 km, 110 km, 120 km, 130 km, 140 km, 150 km, 160 km, 170 km, 180 km, 190 km, 200 km, and 210 km from bus 1 of test transmission line is included in Table 7.

Estimated fault locations for the SPGF, TPG, TPGF, and TLGF events are included in Table 8. The percentage fault location error (FLE) between the actual fault location length (AFL) and the estimated fault location length (EFL) from bus 1 of transmission line for all the fault events is estimated using the below detailed relation:

$$\text{FLE} = \frac{\text{AFL} - \text{EFL}}{\text{AFL}} \times 100\%. \quad (14)$$

Table 8 depicts that the maximum error between AFL and EFL is less than 5% for all types of faults. However, this error is less than 2% when the fault is incident beyond

Table 7: Standard deviation of HSPFI for different fault locations.

S. no.	Line length	Standard deviation of HSPFI			
		SPGF	TPF	TPGF	TLGF
1	10	787782.01	18076862.81	15235630.29	5895450.27
2	20	128124.04	1680012.94	1549542.73	990068.97
3	30	41857.23	491180.74	446918.06	371060.8
4	40	20334.45	212431.08	186918.24	200025.41
5	50	12212.67	92700.57	98809.07	112330.26
6	60	7364.91	54825.23	57025.86	72009.65
7	70	4840.56	34589.45	34885.09	47865.32
8	80	3387.71	24001.58	24237.59	32017.25
9	90	2422.23	16011.58	17064.52	24866.88
10	100	1809.46	10952.21	12083.46	19008.23
11	110	1464.18	8451.23	9106.88	15318.34
12	120	1107.58	6258.52	6681.2	12080.23
13	130	921.82	4833.3	5351.23	9354.6
14	140	755.46	3925.89	4301.23	8200.56
15	150	630.65	3176.7	3391.6	7053.7
16	160	523.25	2602.55	2800.28	6000.64
17	170	438.4	2188.2	2308.8	4904.92
18	180	390.09	1788.2	1938.87	4305.49
19	190	331.05	1466.2	1690.29	3840.51
20	200	290.8	1280.64	1407.42	3350.33
21	210	258.52	1076.3	1227.5	2936.1

Table 8: Fault location estimation and error.

Fault location length (km)	Location of fault event (km)				Error in estimation of line length (%)			
	SPGF	TPF	TPGF	TLGF	SPGF	TPF	TPGF	TLGF
10 km	10.251	9.720	9.748	10.246	−2.509	2.798	2.519	−2.458
20 km	20.296	20.628	20.523	20.823	−1.482	−3.138	−2.613	−4.117
30 km	30.914	30.450	30.768	30.759	−3.046	−1.501	−2.560	−2.530
40 km	40.558	39.708	40.870	39.323	−1.394	0.730	−2.175	1.693
50 km	49.130	51.634	50.301	49.460	1.739	−3.267	−0.601	1.080
60 km	59.424	60.978	60.163	59.022	0.961	−1.630	−0.271	1.630
70 km	69.584	70.554	70.606	69.425	0.594	−0.792	−0.866	0.821
80 km	79.580	79.211	79.497	81.459	0.525	0.986	0.629	−1.823
90 km	90.281	90.046	89.122	90.067	−0.312	−0.051	0.975	−0.075
100 km	100.748	101.554	99.726	100.218	−0.748	−1.554	0.274	−0.218
110 km	109.099	110.243	109.349	109.196	0.819	−0.221	0.592	0.731
120 km	121.174	121.245	120.955	120.006	−0.979	−1.038	−0.796	−0.005
130 km	129.837	131.585	130.024	132.845	0.126	−1.219	−0.018	−2.188
140 km	139.928	140.542	139.611	139.983	0.051	−0.387	0.278	0.012
150 km	149.761	150.290	150.844	148.621	0.159	−0.194	−0.562	0.919
160 km	160.655	160.085	160.556	158.487	−0.409	−0.053	−0.347	0.946
170 km	171.709	169.123	170.972	171.712	−1.005	0.516	−0.572	−1.007
180 km	179.417	180.288	180.978	180.844	0.324	−0.160	−0.543	−0.469
190 km	190.840	191.988	189.249	189.248	−0.442	−1.046	0.395	0.396
200 km	200.375	200.394	200.881	199.804	−0.187	−0.197	−0.440	0.098
210 km	209.441	211.736	210.032	210.566	0.266	−0.826	−0.015	−0.269

60 km from bus 1 of test transmission line. Further, the mean error (%) for the location of SPGF, TPF, TPGF, and TLGF is equal to 0.861, 1.062, 0.859, and 1.092, respectively. Hence, these faults have been located with an accuracy of 99.139%, 98.938%, 99.141%, and 98.908%. Therefore, the proposed protection algorithm locates fault with an average accuracy of 99.031%. Hence, the proposed algorithm is more effective for distant fault locations.

7. Validation of Protection Scheme on Practical Transmission Line of Utility Network

The effectiveness of the protection algorithm is tested on a practical transmission line between 400 kV grid substation (GSS) Bhadla and 400 kV GSS Jodhpur of utility network of Rajasthan Rajya Vidyut Prasaran Nigam Limited (RVPN) in Rajasthan State of India. The technical parameters of this transmission line are described in Table 9.

Table 9: Technical parameters of transmission line.

S. no.	Description of parameter	Magnitude of parameter
1	Line length	215 km
2	Type of conductor	Twin moose
3	Positive sequence resistance	0.029792 Ω/km/ckt
4	Positive sequence reactance	0.332 Ω/km/ckt
5	Positive sequence susceptance ($B/2$)	1.734375×10^{-6} ℧/km/ckt
6	Zero sequence resistance	0.16192 Ω/km/ckt
7	Zero sequence reactance	1.24 Ω/km/ckt
8	Zero sequence susceptance ($B/2$)	1.12×10^{-6} ℧/km/ckt
9	Surge impedance loading (SIL) rating	515 MVA

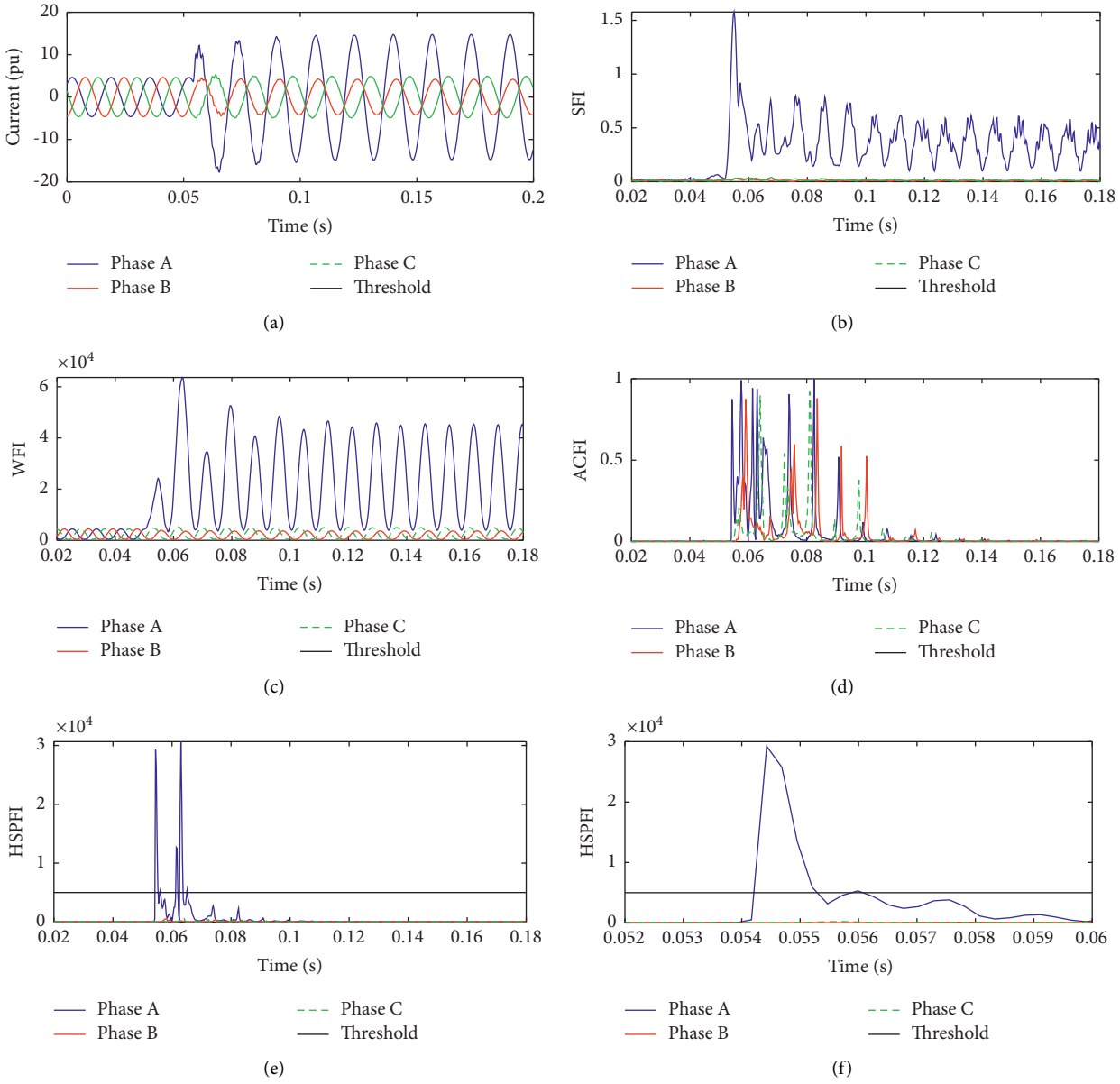

Figure 14: SPGF event on practical test transmission line: (a) current signals, (b) SFI, (c) WFI, (d) ACFI, (e) HSPFI, and (f) high-resolution plot of HSPFI.

Current data are taken from a fault recorder of the line, which indicates that a SPGF event is incident at 0.054167 s and illustrated in Figure 14(a). This current is processed by applying the proposed protection scheme for computing the SFI, WFI, ACFI, and HSPFI, which are described in Figures 14(b)–14(f), respectively.

Table 10: Comparative study of protection algorithms.

S. no.	Attribute	Reference		
		[25]	[26]	Proposed method
1	Signal processing and mathematical techniques employed	WT	HHT and DT	ST, WDF, and ACF
2	Noise level for which algorithm performs effectively	Not investigated	20 dB SNR	10 dB SNR
3	Mean fault location error	1.977%	4.53%	0.968%
4	Fault location accuracy (%)	98.023%	95.47%	99.031%

A high-resolution curve of HSPFI is detailed in Figure 14(f).

Figure 14(a) indicates that current of faulty phase has increased due to the occurrence of SPGF on phase A at 0.054167 s and there is no significant change in the current of healthy phases A and B. Figure 14(b) indicates that the magnitude of SFI for faulty phase A has increased due to the occurrence of SPGF and the magnitude of this index for healthy phases is nearly zero. Figure 14(c) elaborates that the magnitude of WFI for faulty phase A has increased due to the occurrence of fault and this magnitude for healthy phases remains nearly zero. Figure 14(d) illustrates that peaks of unit magnitude are associated with the ACFI plot of faulty phase A and ACFI remains near zero for healthy phases. Figure 14(e) indicates that the magnitude of HSPFI for faulty phase A has crossed the threshold (TH) just after fault occurrence. However, due to the occurrence of fault the magnitude of HSPFI for healthy phases is lower than the threshold. Hence, the SPGF is identified effectively by the application of HSPFI. It is inferred from the high-resolution plot of HSPFI described in Figure 14(f) that the SPGF event has been detected in a time duration of 0.00067 s. Hence, the proposed algorithm has effectively detected a fault event on a practical transmission line of large area utility network of RVPN.

8. Performance Comparative Study

The performance of designed protection scheme is compared with the wavelet-based protection scheme [25] and HHT-based protection scheme [26]. These algorithms detect the fault in a time interval of a quarter cycle, whereas the proposed hybrid signal processing protection scheme based on ST, WDF, and ACF detects the fault in a time interval of $(1/27)^{th}$ part of a cycle. Hence, the designed protection scheme is 7 times faster relative to protection schemes reported in [25, 26]. Further, the performance of HHT-based fault detection and decision tree (DT)-based fault classification algorithm reported in [26] is only 91.20% with 20 dB SNR noise and further decreases for noise of 10 dB SNR and the performance of wavelet-based protection scheme [25] is deteriorated for noise levels higher than 30 dB SNR. However, designed HSPFI detects the faults with 100% accuracy even with high noise levels of 10 dB SNR. A comparative study of the techniques is provided in Table 10.

9. Conclusions

This study introduced a hybrid transmission line protection scheme using current features computed by the application of ST, WDF, and alienation coefficient to detect fault events and statistical formulation for fault location. Fault classification is achieved considering the number of faulty phases and hybrid ground fault index, which is based on features of zero sequence current computed using ST and WDF. It is concluded that the proposed hybrid signal processing algorithm effectively detected all types of faults such as SPGF, TPF, TPGF, TLF, and TLGF in a time duration of 0.0006 s. The algorithm successfully detected these faults during the scenario of fault impedance variation, variable sampling frequency, variations in angle of fault incidence, reverse power flow on transmission line, highly loaded line, different fault locations online, and noisy conditions. Faults are located on the line with a maximum error of less than 5%. The mean error (%) for the location of SPGF, TPF, TPGF, and TLGF is equal to 0.861, 1.062, 0.859, and 1.092, respectively. Hence, these faults have been located with an accuracy of 99.139%, 98.938%, 99.141%, and 98.908%. Therefore, the proposed protection algorithm locates faults on transmission line with an average accuracy of 99.031%. The designed protection algorithm effectively detected the faults on a practical transmission line of RVPN utility grid. The proposed algorithm performs better than the HHT-based protection scheme and WT-based protection algorithm available in the literature in terms of mean error of fault location, fault location accuracy, and noise level. Further, the performance of protection scheme is also high even in the noisy environment with 10 dB SNR noise level.

Abbreviations

ACF: Alienation coefficient
ACFI: Alienation coefficient fault index
AFL: Fault location length
CB: Circuit breaker
CC: Correlation coefficient
CT: Current transformer
DFT: Discrete Fourier transform
DPMI: Derived phase mean index
DWT: Discrete wavelet transform
EFL: Estimated fault location length
FACTS: Flexible AC transmission system
FLE: Fault location error
GFD: Global fault detector
GSS: Grid substation
STH: Ground threshold
HGFI: Hybrid ground fault index
HHT: Hilbert–Huang transform
HIF: High impedance faults
HSPFI: Hybrid signal processing fault index

HSTLP: Hybrid scheme for transmission line protection
HWF: Hybrid weight factor
MSTI: Median ST index
PMI: Phase mean index
PMU: Phasor measurement unit
PSO: Particle swarm optimization
RVPN: Rajasthan Rajya Vidyut Prasaran Nigam Limited
SAT-CNN: Self-attention convolution neural network
SFI: Stockwell fault index
SGFI: Stockwell ground fault index
SIL: Surge impedance loading
SNR: Signal-to-noise ratio
SPGF: Single-phase-to-ground fault
ST: Stockwell transform
TH: Threshold
TL: Transmission line
TLF: Three-line fault
TLGF: Three-line-to-ground fault
TPF: Two-phase fault
TPGF: Two-phase-to-ground fault
UG: Utility grid
VSTI: Variance ST index
WDF: Wigner distribution function
WFI: Wigner fault index
WGFI: Wigner ground fault index
WT: Wavelet transform.

Data Availability

For the data-related queries, kindly contact Anup Kumar, anupchirag@gmail.com.

Conflicts of Interest

The authors declare that there are no conflicts of interest.

Authors' Contributions

A.K. conceptualized the study, designed methodology, investigated the study, and wrote and prepared the original draft; A.K. and O.P.M. provided software, validated the data, involved in formal analysis, and curated the data; H.S. and R.N.M. provided resources and supervised the data; A.K., O.P.M., H.S., and R.N.M. wrote, reviewed, and edited the manuscript; H.S., R.N.M., and B.K. visualized the data; and all authors have read and agreed to the published version of the manuscript.

References

[1] R. K. Goli, A. Gafoor Shaik, and S. S. Tulasi Ram, "A transient current based double line transmission system protection using fuzzy-wavelet approach in the presence of UPFC," *International Journal of Electrical Power & Energy Systems*, vol. 70, pp. 91–98, 2015.

[2] S. Jangir, R. Choudhary, B. Rathore, and A. G. Shaik, "Transmission line fault detection and classification using alienation coefficient technique for current signals," in *Proceedings of the 2018 3rd International Conference for Convergence in Technology (I2CT)*, pp. 1–6, Pune, India, April 2018.

[3] B. R. Kumar, A. Mohapatra, S. Chakrabarti, and A. Kumar, "Phase angle-based fault detection and classification for protection of transmission lines," *International Journal of Electrical Power & Energy Systems*, vol. 133, Article ID 107258, 2021.

[4] S. R. Fahim, Y. Sarker, S. K. Sarker, M. R. I. Sheikh, and S. K. Das, "Self attention convolutional neural network with time series imaging based feature extraction for transmission line fault detection and classification," *Electric Power Systems Research*, vol. 187, Article ID 106437, 2020.

[5] C. D. Prasad and P. K. Nayak, "Performance assessment of swarm-assisted mean error estimation-based fault detection technique for transmission line protection," *Computers & Electrical Engineering*, vol. 71, pp. 115–128, 2018.

[6] T. R. Althi, E. Koley, and S. Ghosh, "Fuzzy logic based fault detection and classification scheme for series faults in six phase transmission line," in *Proceedings of the 2021 7th International Conference on Electrical Energy Systems (ICEES)*, pp. 479–483, Chennai, India, February 2021.

[7] H. A. Abd el-Ghany, I. A. Soliman, and A. E. ELGebaly, "An advanced wide-area fault detection and location technique for transmission lines considering optimal phasor measurement units allocation," *Alexandria Engineering Journal*, vol. 61, no. 5, pp. 3971–3984, 2022.

[8] A. M. El-Zonkoly and H. Desouki, "Wavelet entropy based algorithm for fault detection and classification in FACTS compensated transmission line," *International Journal of Electrical Power & Energy Systems*, vol. 33, no. 8, pp. 1368–1374, 2011.

[9] S. R. Fahim, S. K. Sarker, S. M. Muyeen, S. K. Das, and I. Kamwa, "A deep learning based intelligent approach in detection and classification of transmission line faults," *International Journal of Electrical Power & Energy Systems*, vol. 133, Article ID 107102, 2021.

[10] M. Khoshbouy, A. Yazdaninejadi, and T. G. Bolandi, "Transmission line adaptive protection scheme: a new fault detection approach based on pilot superimposed impedance," *International Journal of Electrical Power & Energy Systems*, vol. 137, Article ID 107826, 2022.

[11] R. Resmi, V. Vanitha, E. Aravind, B. R. Sundaram, C. R. Aswin, and S. Harithaa, "Detection, classification and zone location of fault in transmission line using artificial neural network," in *Proceedings of the 2019 IEEE International Conference on Electrical, Computer and Communication Technologies (ICECCT)*, pp. 1–5, Coimbatore, India, February 2019.

[12] S. Belagoune, N. Bali, A. Bakdi, B. Baadji, and K. Atif, "Deep learning through LSTM classification and regression for transmission line fault detection, diagnosis and location in large-scale multi-machine power systems," *Measurement*, vol. 177, Article ID 109330, 2021.

[13] S. Das, S. P. Singh, and B. K. Panigrahi, "Transmission line fault detection and location using wide area measurements," *Electric Power Systems Research*, vol. 151, pp. 96–105, 2017.

[14] A. R. Singh, N. R. Patne, and V. S. Kale, "Synchronized measurement based an adaptive distance relaying scheme for STATCOM compensated transmission line," *Measurement*, vol. 116, pp. 96–105, 2018.

[15] K. R. Dhenuvakonda, A. Singh, M. P. Thakre, R. R. Karasani, and R. Naidoo, "Adaptive digital distance relay for SSSC-based double-circuit transmission line using phasor

measurement unit," *International Transactions on Electrical Energy Systems*, vol. 29, no. 4, Article ID e2787, 2019.

[16] A. R. Singh, N. R. Patne, and V. S. Kale, "Adaptive distance protection setting in presence of mid-point STATCOM using synchronized measurement," *International Journal of Electrical Power & Energy Systems*, vol. 67, pp. 252–260, 2015.

[17] A. R. Singh and S. S. Dambhare, "Adaptive distance protection of transmission line in presence of SVC," *International Journal of Electrical Power & Energy Systems*, vol. 53, pp. 78–84, 2013.

[18] A. R. Singh, N. R. Patne, V. S. Kale, and P. Khadke, "Digital impedance pilot relaying scheme for STATCOM compensated TL for fault phase classification with fault location," *IET Generation, Transmission & Distribution*, vol. 11, no. 10, pp. 2586–2598, 2017.

[19] B. Rathore and A. G. Shaik, "Wavelet-alienation based transmission line protection scheme," *IET Generation, Transmission & Distribution*, vol. 11, no. 4, pp. 995–1003, 2017.

[20] S. R. Ola, A. Saraswat, S. K. Goyal, S. K. Jhajharia, B. Rathore, and O. P. Mahela, "Wigner distribution function and alienation coefficient-based transmission line protection scheme," *IET Generation, Transmission & Distribution*, vol. 14, no. 10, pp. 1842–1853, 2020.

[21] R. Arranz, Á. Paredes, A. Rodríguez, and F. Muñoz, "Fault location in transmission system based on transient recovery voltage using Stockwell transform and artificial neural networks," *Electric Power Systems Research*, vol. 201, Article ID 107569, 2021.

[22] L. Čurović, J. Murovec, T. Novaković, R. Prislan, and J. Prezelj, "Stockwell transform for estimating decay time at low frequencies," *Journal of Sound and Vibration*, vol. 493, Article ID 115849, 2021.

[23] N. Ali Khan, I. Ahmad Taj, M. Noman Jaffri, and S. Ijaz, "Cross-term elimination in Wigner distribution based on 2D signal processing techniques," *Signal Processing*, vol. 91, no. 3, pp. 590–599, 2011.

[24] B. Rathore and A. G. Shaik, "Wavelet-alienation based protection scheme for multi-terminal transmission line," *Electric Power Systems Research*, vol. 161, pp. 8–16, 2018.

[25] A. G. Shaik and R. R. V. Pulipaka, "A new wavelet based fault detection, classification and location in transmission lines," *International Journal of Electrical Power & Energy Systems*, vol. 64, pp. 35–40, 2015.

[26] M. Shaik, A. G. Shaik, and S. K. Yadav, "Hilbert-Huang transform and decision tree based islanding and fault recognition in renewable energy penetrated distribution system," *Sustainable Energy, Grids and Networks*, vol. 30, Article ID 100606, 2022.